Near-threshold photoassociation of $^{87}Rb_2$

M. Kemmann,* I. Mistrik, S. Nussmann,† and H. Helm
Department of Molecular and Optical Physics, Albert-Ludwigs-Universität, Hermann-Herder-Strasse 3, D-79104 Freiburg, Germany

C. J. Williams and P. S. Julienne
National Institute of Standards and Technology, 100 Bureau Drive, Stop 8423, Gaithersburg, Maryland 20899-8423, USA
(Received 7 May 2003; published 26 February 2004)

Photoassociation of cold $^{87}Rb(5s,f_b=2)$ atom pairs is studied within 13 GHz of the dissociation limits $^{87}Rb(5p_{3/2},f_a)+{}^{87}Rb(5s,f_b=2)$. Vibrational levels in the long range, hyperfine manifolds of the 0_g^- and 1_g states arising from the $^{87}Rb(5p_{3/2})$ fine structure limit are identified to lead to the formation of stable molecules in the photoassociation process. The vibrational bands are observed to break off, at positions matching the energetic location of potential-energy barriers predicted in the hyperfine manifolds at about 1 GHz above the $^{87}Rb(5p_{3/2},f_a=3)+{}^{87}Rb(5s,f_b=1)$ dissociation limit. Empiricial potential-energy curves are derived from the data. These are found to be in agreement with predictions based on the long-range hyperfine recoupling of the excited molecular states. The selectivity of the excitation process and predissociation mechanisms are discussed.

DOI: 10.1103/PhysRevA.69.022715 PACS number(s): 34.20.Cf, 32.70.Cs, 32.80.Pj

I. INTRODUCTION

Photoinduced association [1] of laser-cooled atoms as a source of translationally cold molecules has been extensively studied in recent years [2–10]. This topic has also received detailed attention from theory [11]. Spontaneous and stimulated decay of photoexcited long-range collision pairs can lead to the formation of stable bound states of translationally cold molecules. In the absence of a photoassociation (PA) laser, formation of stable molecules is observed in cold atom environments as a consequence of three-body recombination and of PA by the trapping and repumping lasers in a magneto-optic trap (MOT) [5].

Here we report experiments on the formation of $^{87}Rb_2$ molecules following photoexcitation of cold collision pairs to energies very close to the $^{87}Rb(5p_{3/2})+{}^{87}Rb(5s_{1/2})$ dissociation limits. Figure 1 shows the long-range excited-state potential-energy curves [12] that arise from the fine-structure dissociation limits $^{87}Rb(5p)+{}^{87}Rb(5s)$. The energy region studied here (-2 to -13 GHz) falls in the immediate vicinity of zero on the energy scale in Fig. 1. Vibrational identification of the photoassociation spectra allows us to derive portions of the long-range potential-energy curves at atom separations of $\approx 200a_0$ ($1a_0=0.0529$ nm). We compare these curves with calculated $^{87}Rb_2$ adiabatic hyperfine potential-energy curves that are based on the long-range properties of two ^{87}Rb atoms. The photoassociation spectra show a breakoff of vibrational progressions due to hyperfine interactions.

II. EXPERIMENT

The photoassociation experiment is carried out in a vapor-loaded MOT with time-of-flight spectrometer for ion mass analysis [13]. The MOT is operated at a field gradient of 1.4 mT/cm with a ^{87}Rb reservoir at room temperature (≈ 297 K). Two phase-locked and amplified diode lasers are used, one to drive the cooling transition of the MOT and one to scan the photoassociation spectrum. An independently stabilized laser is used for the atomic repumping cycle. The photoassociation laser is kept at a variable detuning from the cooling laser by employing a digital phase-lock loop as introduced by Prevedelli *et al.* [14] and described in Ref. [15]. The beams of the cooling and PA laser are merged in parallel linear polarization and are fed into the three mutually orthogonal arms of the MOT where they counterpropagate in σ^+-σ^- configuration. Each arm carries an intensity of ≈ 10 mW from each laser, at $1/e^2$ laser beam diameters of $2r_0=10$ mm.

Photoassociation events which are followed by spontaneous decay of $^{87}Rb_2^*$ to stable bound states are detected by photoionization of the stable molecules. $^{87}Rb_2^+$ was formed with a weakly focussed dye laser at wavelengths near 600 nm and counted after mass selection. We approximately matched the size of the cold atom cloud with the cross section of the ionization laser beam (30 Hz repetition rate, pulse duration 7 ns, pulse energy 1-4 mJ). Ionization of the molecule was found to saturate at an intensity lower than that required to saturate off-resonance three-photon ionization of ground-state atoms. We take this as indication that two photons suffice for ionization of the molecules. This suggests that neutral $^{87}Rb_2$ detected here is primarily formed in high vibrational levels of the ground (presumably $a^3\Sigma_u^+$) state in the PA process. We continuously operate the trap while recording the PA spectrum.

While keeping the ionization laser at the fixed wavelength $\lambda_{air}=604.6$ nm, the photoassociation spectrum in ^{87}Rb was recorded by detuning the PA laser from -2 to -13 GHz from the atomic transition

$$^{87}Rb(5s,f_b=2)+\hbar\omega_0 \rightarrow {}^{87}Rb(5p_{3/2},f_a=3). \quad (1)$$

*Present address: FOM institute AMOLF, Amsterdam, The Netherlands.

†Present address: MPQ, Garching, Germany.

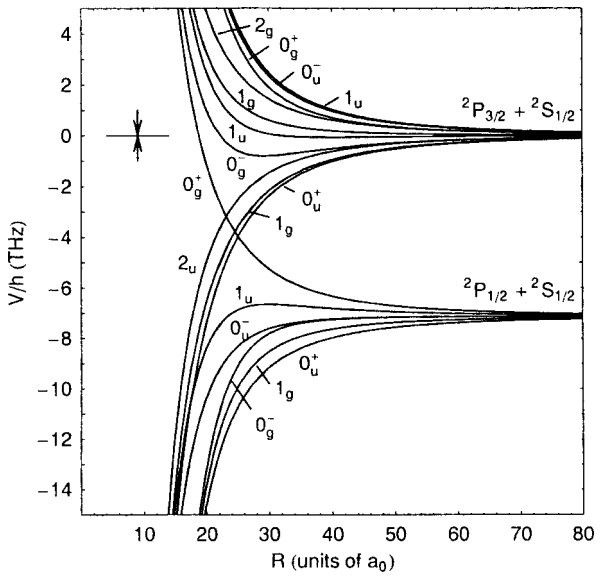

FIG. 1. Long-range potential-energy curves [12] arising from the lowest excited-state dissociation limit of Rb_2. The photoassociation spectrum reported here covers a narrow range near zero energy, as indicated by arrows.

Cold trapped ground-state ^{87}Rb atoms with the hyperfine quantum number $f_b=2$ are observed to photoassociate in the process

$$^{87}\mathrm{Rb}(5s,f_b=2)+{}^{87}\mathrm{Rb}(5s,f_b=2)+\hbar\omega\rightarrow{}^{87}\mathrm{Rb}_2^*. \quad (2)$$

The restriction to $f_b=2$ is dictated by the choice of the wavelengths of the PA laser in reaction (2) as will be discussed below. Molecules formed as a consequence of this excitation process were photoionized and this signal was recorded as a function of ω. This photoassociation spectrum is shown in Fig. 2. This spectrum was recorded at a stepsize of 10 MHz, accumulating at each wavelength the counts from 200 shots of the ionization laser. At the highest peaks about one ionized molecule per laser shot is detected due to photoassociation. A continuous background of spontaneously formed $^{87}Rb_2$ molecules appears in the spectrum. The ionization signal from spontaneously formed $^{87}Rb_2$ amounts to ≈ 0.4 ions per laser shot.[1] We observe spontaneous formation of $^{87}Rb_2$ and $^{85}Rb_2$ molecules at about equal rates, when operating the trap in ^{87}Rb and ^{85}Rb, respectively. Figure 3 shows wavelength scans for photoionization of the spontaneously formed molecules. These spectra closely resemble the spectra reported by Gabbanini *et al.* [8]. We find that in this wavelength region the photoionization spectrum of $^{87}Rb_2$ molecules formed in process (2) is identical to that observed for molecules formed spontaneously.[2]

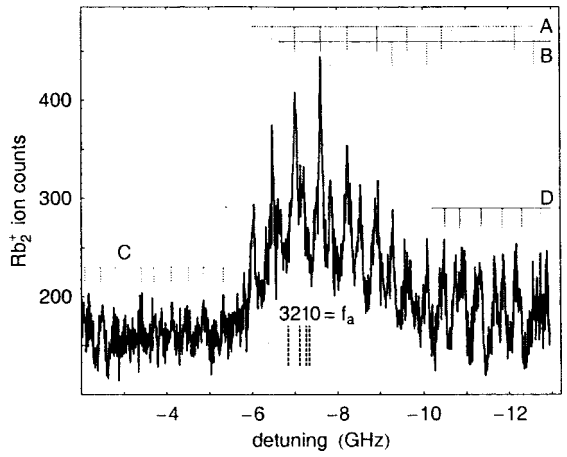

FIG. 2. Photoassociation spectrum leading to stable $^{87}Rb_2$ molecules. The detuning is red of the dissociation limit $(5p_{3/2},f_a=3)+(5s,f_b=2)$. The dashed vertical lines give the energetic location of the $(5p_{3/2},f_a=0-3)+(5s,f_b=1)$ limits.

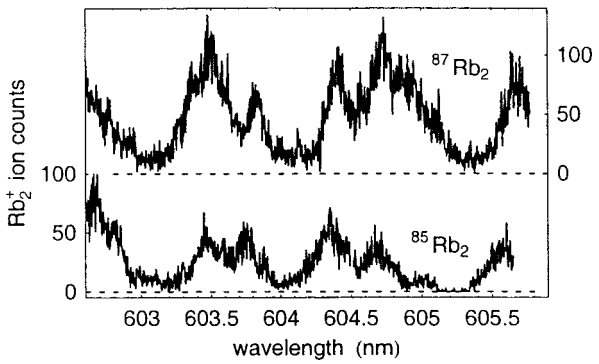

FIG. 3. Photoionization spectra of spontaneously formed Rb_2 molecules.

We recorded the trap flourescence spectrum simultaneously with the ionization spectrum. As is evident from Fig. 4, the fluorescence spectrum displays much more complex spectral features than the ionization spectrum. This increased complexity is to be expected since the laser excites a number of other levels that lead to trap loss but not to molecule formation.

Selected portions of the spectra were studied at a stepsize of 1 MHz. The narrowest spectral features were found to be around 20 MHz wide, but limitations due to poor counting statistics make this value uncertain. The sum of temperature, Zeeman, and natural broadening is expected to be in the range of ≈ 10 MHz. Additional broadening is likely due to unresolved hyperfine structure [16]. Without doubt both spectra will reveal much richer substructures once the signal-to-noise level is improved.

III. SPECTRAL IDENTIFICATION

The dashed vertical lines in Fig. 2 indicate the energetic location of the four hyperfine dissociation limits

[1]When using an excimer-pumped dye laser at a repetition rate of 150 Hz and comparable pulse energy we observed comparable ion count rates. This suggests that molecules are being lost from the region of formation at a rate faster than about 10 ms. Based on this loss rate we estimate the rate of spontaneous formation of $^{87}Rb_2$ molecules in the trap to exceed 400 s^{-1}.

[2]In the experiment described in Ref. [8] formation of $^{87}Rb_2$ was only observed in the presence of the PA laser.

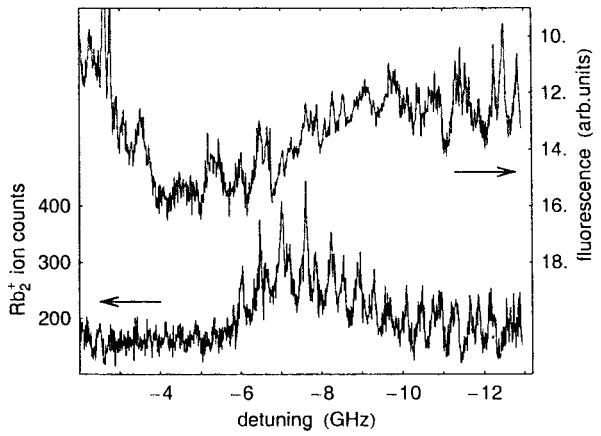

FIG. 4. Comparison of the photoassociation spectrum with the trap fluorescence spectrum. The trap fluorescence intensity is shown inverted.

$^{87}Rb(5p_{3/2}, f_a=0,1,2,3) + {}^{87}Rb(5s, f_b=1)$. The dominant features in the PA spectrum end abruptly at a detuning of about -6 GHz below $^{87}Rb(5p_{3/2}, f_a=3) + {}^{87}Rb(5s, f_b=2)$, at an energy *above* the four asymptotes belonging to $f_b=1$. Only weak features appear in the spectrum at smaller detunings. We identify the main peaks in the spectrum as members of four vibrational series which we label *A*, *B*, *C*, and *D*. The energetic location of vibrational members in these series is marked above the experimental spectrum in Fig. 2. Several peaks show substructure, specifically at larger detuning where a number of peaks remain unidentified.

In order to deduce the long-range shape and location of potential-energy curves which support the regular pattern of vibrational peaks observed, we fitted the peak positions of series *A* and *B* using the LeRoy-Bernstein formalism [17]. In this approach the long-range potential is approximated by a simple power law with the energy

$$V_3(R) = E_d - \frac{C_3^{eff}}{R^3}, \tag{3}$$

where R is the internuclear separation. The fit parameters C_3^{eff} and E_d, together with the limiting vibrational level v_d at threshold, define the vibrational energy relative to the dissociation limit [17]

$$E_v = -\left[\frac{(v_d - v)}{\sqrt[3]{C_3^{eff}}}\frac{\hbar}{2}\sqrt{\frac{2\pi}{\mu}}\frac{\Gamma\left(\frac{4}{3}\right)}{\Gamma\left(\frac{5}{6}\right)}\right]^6, \tag{4}$$

where μ is the reduced mass of the molecule. Effective potential-energy curves obtained in this way are defined only at the right-hand turning points of the observed vibrational levels. These effective potential-energy curves are shown in Fig. 5 together with the vibrational levels used in the fit. Also shown in this figure by diamonds are the highest vibrational levels determined for the 0_g^- state in Ref. [10]. The weaker series *C* and *D* are poorly defined and do not warrant a meaningful fit at the current level of resolution. The fit parameters obtained for series *A* and *B* are listed in Table I.

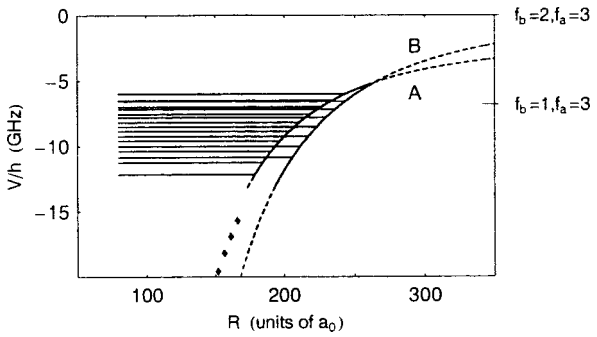

FIG. 5. The empirical potential-energy curves for series *A* and *B* are shown together with the vibrational levels observed. The diamonds indicate the right-hand turning points determined for the highest vibrational levels of the 0_g^- state in Ref. [10] ($v=68$–71).

Note that the parameters in this table do not redefine the C_3 coefficient appropriate for the resonant dipole interaction between $^{87}Rb(5p) + {}^{87}Rb(5s)$, rather these parameters approximate the *portion* of the adiabatic hyperfine potentials near the right-hand turning points of the observed vibrational levels. Outside the fitted range (column 5 in Table I), the shape of the real potentials may deviate drastically from that given by the restricted curvature permitted in Eq. (3). For the same reason the fitted dissociation energy E_d (column 3 in Table I) has no physical meaning.[3] We see from Fig. 5 that the observed levels have right-hand turning points at around $200a_0$.

In our spectral analysis we have neglected the rotational energy associated with the mechanical rotation of the internuclear axis (see the following Section). To first order the rotational energy weakly broadens the spectral features and causes a small overall shift. Due to the huge internuclear separation, the rotational constant $B_v = \langle \hbar^2/(2\mu R^2) \rangle$ has a magnitude on the order of only 1 MHz. Because of the low temperature in a MOT, only a few units of rotational energy can be excited so that rotational structure is unresolved in our features.

IV. COMPARISON WITH THEORY

We have calculated the adiabatic hyperfine potential-energy curves of the nonrotating $^{87}Rb_2$ dimer molecule in a body-fixed frame. At long range these are well determined from a knowledge of the atomic fine- and hyperfine-structure energy levels and the strength of the dipole-dipole interaction proportional to d_z^2/R^3. Here $d_z^2 = 8.938$ a.u. for ^{87}Rb (see Table II in Ref. [18]) is the projection of the atomic transition dipole on some quantization axis $\vec{z}$. We first set up the dimer Hamiltonian in a basis set comprised of states of total electronic-spin angular momentum $\vec{f}$, where

[3]The $^{87}Rb(5p_{3/2}, f_a=3) + {}^{87}Rb(5s, f_b=1)$ limit corresponds to $E_d=0$.

TABLE I. Fit parameters of Eq. (3), where C_3 is given in atomic units (1 a.u.$=0.646$ ZJ nm^3). The last two columns give the theoretical states which most closely fit the empirical potential-energy curves.

	C_3^{eff} (a.u.)	v_d	E_d/h GHz	Range (units of a_0)	hf-labeled states	Case c state
A	8.85	-0.163	-1.98	170–240	12(0b1), 18(1a)	$0g^-$
B	14.39	-0.061	-0.007	200–240	12(0a1), 20(1b)	$1g$

$$\vec{f}=\vec{\ell}_a+\vec{s}_a+\vec{i}_a+\vec{s}_b+\vec{i}_b \tag{5}$$

is the sum of electron orbital $\vec{\ell}_a$, electron spin *s*, and nuclear spin *i* of the two atoms (atom *a* is taken to be the excited atom and *b* the ground state).[4] We find the adiabatic potential-energy curves by diagonalizing the Hamiltonian. The Hamiltonian ignoring mechanical rotation is diagonal in the projection ϕ of $\vec{f}$ on the internuclear axis, that is, states that differ in ϕ quantum numbers are not coupled.

It is also possible to take into account the mechanical rotation $\vec{l}$ of the molecular axis to give eigenstates of the total angular momentum $\vec{F}=\vec{f}+\vec{l}$ and total molecular parity including inversion of $\vec{l}$. These are the eigenstates that would be measured in an experiment. As we noted in the preceding section, the rotational energy is small enough for our present spectrum to ignore. The mechanical rotation also gives rise to weak Coriolis-like forces in the body-fixed frame that we also ignore here. These can cause *F*-dependent avoided crossings between states of different ϕ.

For the $^{87}Rb_2$ dimer there are a total of 384 distinct basis functions which are needed to define the Hamiltonian matrix from which the adiabatic potential curves are calculated. The resulting eigenstates exhibit parity with respect to inversion of all electronic and spin coordinates in the body-fixed frame. Since nuclear spin interactions can mix electronic states of different *gerade* or *ungerade* symmetry, only total parity, not electronic parity alone, is a good quantum number for labeling eigenstates. We designate + and – parity as $p=a$ and *b*, respectively ($\phi=0$ states also exhibit + or – Kronig symmetry with respect to reflection in a plane containing the internuclear axis; we denote this symmetry by the index $r=1$ or 2 for $\phi=0$ states). Consequently, the adiabatic potential curves can be labeled by the quantum numbers $j(0pr)$ for nondegenerate $\phi=0$ states and $j(\phi p)$ for the doubly degenerate $\phi\neq 0$ states, where *j* is a counting index that identifies the unique roots of each symmetry. Note that $^{85}Rb_2$ has 864 distinct basis functions due to the higher nuclear spin quantum number.

In order to facilitate the following discussion we show in Fig. 6 all molecular states of positive parity that arise from $^{87}Rb(^2P_{3/2})+{}^{87}Rb(^2S_{1/2})$ at three different sets of magnification. (Note that the energy scale in Fig. 1 is in units of 1000 GHz). A similar looking set of potentials exists for states of negative electronic-spin parity.

In Figs. 7 and 8 we compare the empirically derived sections of long-range potentials with the theoretical curves which most closely match the empirical curves. These are the states 12(0b1) and 18(1a) for series *A* and the states 12(0a1), and $20(1b)$ for series *B*. The number *j* in front of the bracket counts from the lowest-energy state of the $^{87}Rb(5p)+{}^{87}Rb(5s)$ manifold.

V. DISCUSSION

In view of the complexity and large number of potential-energy curves predicted, it may at first appear surprising that the experimental photoassociation spectrum is rather simple and restricted to only a few vibrational series. In spite of the large number of potential-energy curves that originate from the hyperfine dissociation limits of $^{87}Rb(5p_{3/2})+{}^{87}Rb(5s_{1/2})$, only selected theoretical hyperfine potentials match the empirical data. These are potentials which at intermediate atomic separations form the hyperfine manifolds of states of 0_g^- and 1_g symmetry and which correlate to $^{87}Rb(5p_{3/2})+{}^{87}Rb(5s_{1/2})$ (see Fig. 1). At molecular distances these 0_g^- states merge into the $\Omega=0$ component of the repulsive $^3\Pi_g$ state, while the 1_g states merge into the $\Omega=1$ component of the $^3\Pi_g$ state [19].

The experimentally observed vibrational structure in series *A* and *B* is inconsistent with potentials that correlate to the weakly attractive 1_u states (these evolve into the attractive $^1\Pi_u$ state at molecular distances). It is also inconsistent with any of the long-range attractive potential-energy curves (1_g and 0_u^+) which adiabatically emerge from the hyperfine dissociation limits $^{87}Rb(5p_{3/2},f_a)+{}^{87}Rb(5s,f_b=1)$.

Selectivity to a few favored states, as is observed here, arises first of all in the excitation process of the cold collision pair. At internuclear separations of $\approx 200a_0$ the transition moments favor excitation of the 0_g^-, 0_u^+, and 1_g states [20]. The photoassociation spectrum (as opposed to the trap-loss spectrum shown in the top of Figure 4) has imprinted additional selectivity from the dynamics of the excited molecular state. The probability for bound-bound emission to form a stable $^{87}Rb_2$ molecule and the probability for predissociation govern the spectral appearance of the molecular ion signal in Figure 2. Because only $^3\Sigma_u^+$ states appear to be readily ionized, the states that predominate in the PA ionization spectrum must be of *gerade* symmetry.

An additional selectivity of molecular states which contribute to our PA spectrum arises from the fact that, at the internuclear separations important here, states which diabati-

[4]We assume here for labeling purposes that atom *a* is the ^2P state atom and atom *b* is the ^2S state atom (i.e., $l_b=0$), even though the total state is fully symmetric.

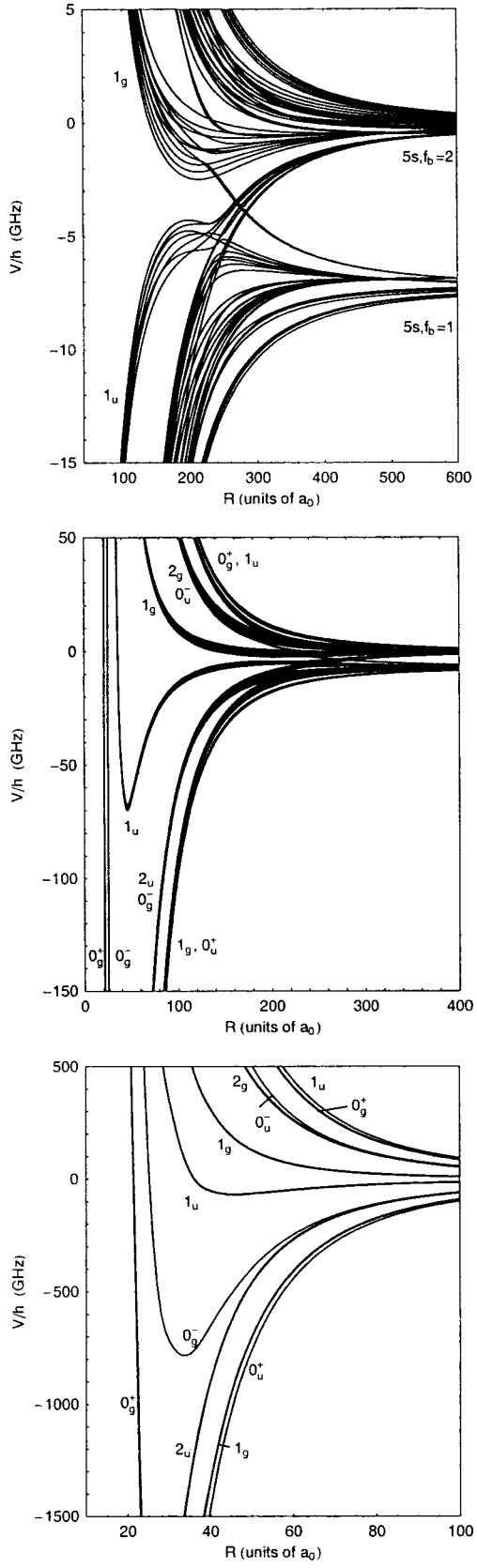

FIG. 6. Hyperfine potential-energy curves of $^{87}Rb_2$ with parity a (see text) near the $(5p_{3/2}+5s_{1/2})$ limits are shown at three different magnifications.

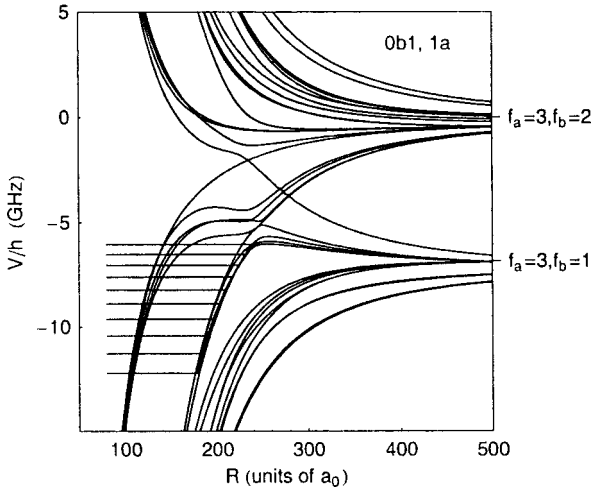

FIG. 7. The empirical potential-energy curve for series A is shown together with the predicted hyperfine states of $(0b1)$ and $(1a)$ symmetry.

cally evolve into the dissociation limit $^{87}\mathrm{Rb}(5p_{3/2})+{}^{87}\mathrm{Rb}(5s,f_b=1)$ are unfavorable in photoexcitation from $(5s,f_b=2)+(5s,f_b=2)$ collision pairs. Excitation of such states requires a hyperfine-changing process in one of the $^{87}\mathrm{Rb}(5s)$ atoms concurrent with electronic excitation of the other atom. Given this reasoning and the wavelength range chosen here we expect the vibrational peaks in our spectrum to arise from potential-energy curves which derive their dominant state amplitude from the $^{87}\mathrm{Rb}(5p_{3/2})+{}^{87}\mathrm{Rb}(5s,f_b=2)$ limits. The fitted potentials for series A and B indeed bear this out. The closest match of the series is to potential-energy curves which extrapolate to the favorable $^{87}\mathrm{Rb}(5p_{3/2})+{}^{87}\mathrm{Rb}(5s,f_b=2)$ asymptotes.

In order to explore the origin of the enhanced photoassociation near threshold we calculated the free-bound absorption probability from collision pairs with kinetic energies between 1 and 30 MHz above the $^{87}\mathrm{Rb}(5s,f_b=2)$

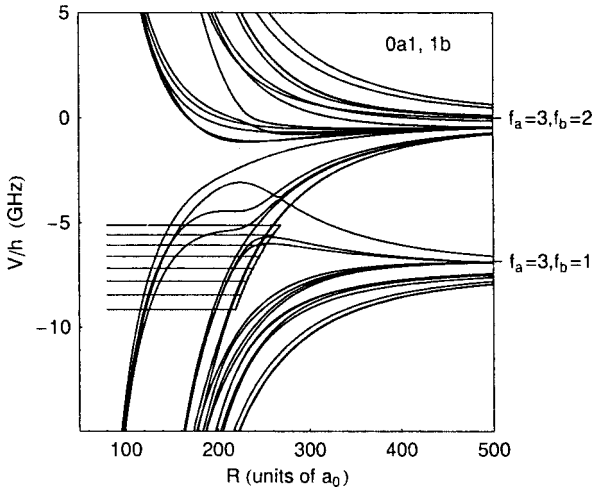

FIG. 8. The empirical potential-energy curve for series B is shown together with the predicted hyperfine states of $(0a1)$ and $(1b)$ symmetry.

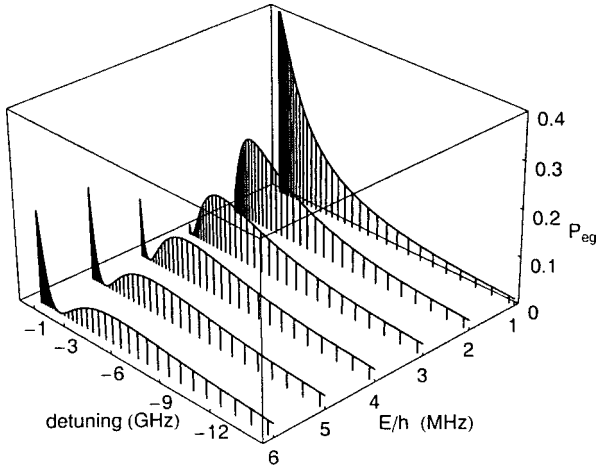

FIG. 9. Free-bound absorption probability as a function of the detuning from the dissociation limit and of the continuum energy E of the collision pair.

$+ {}^{87}\mathrm{Rb}(5s, f_b=2)$ asymptote. Note that the observed temperature in our MOT ($\approx 100\ \mu$K) corresponds to a collision energy of ≈ 2 MHz. The reflection approximation [21–23] is adequate in this domain of energy and detuning. The free-bound absorption probability is proportional to the square of the ground-state wave function at the Condon point, which is the internuclear separation where the difference between the ground- and excited-state potential-energy curves matches the photon energy. The absorption probability, as defined by Eq. (35) of Ref. [24], is shown in Fig. 9 for an assumed ground-state scattering length of $99a_0$ [25]. Transitions from cold collision pairs to the highest vibrational levels of the long-range attractive states are modulated by this dependence on detuning. The weak modulation predicted in the free-bound absorption cross section is not the origin for the abrupt breakoff of series A and B near a detuning of -6 GHz.[5]

The observed vibrational series A and B break off at energies above the ${}^{87}\mathrm{Rb}(5p_{3/2}) + {}^{87}\mathrm{Rb}(5s, f_b=1)$ limits which by the argument given above are unfavorable for direct excitation. We attribute this breakoff to hyperfine predissociation of the bound states to the ${}^{87}\mathrm{Rb}(5p_{3/2}) + {}^{87}\mathrm{Rb}(5s, f_b=1)$ limits, and/or the formation of maxima in the adiabatic potentials owing to hyperfine recoupling of the Hund's case c states. Numerous avoided crossings are apparent in the theoretical potentials near the dissociation limit, as seen in Fig. 6. The avoided crossings lead to barriers in the potential energy, very close in energy to the observed breakoff of bands.

The predissociation argument may be further explored, as molecular states belonging to the same ϕ value interact with each other by radial coupling. Hence excitation to states which adiabatically continue to the ${}^{87}\mathrm{Rb}(5p_{3/2}) + {}^{87}\mathrm{Rb}(5s, f_b=2)$ asymptotes can be subject to predissociation by radial coupling. Molecular states of different ϕ values are coupled to each other by the weaker interactions between the spins, and between the spins and the orbital momentum, the selection rule being $\Delta\phi = \pm 1$. While the sudden termination of series A and B is consistent the appearance of barriers in the respective adiabatic potential-energy curves or with predissociation by states of its kind with $(\Delta\phi = 0)$, numerous other potential-energy curves with $(\Delta\phi = \pm 1)$ exist which have barriers at the energy of the observed break off (see Fig. 6).

Molecular dynamics in the dense region of hyperfine states near the excited-state dissociation limit is clearly complex and, when looked at in more detail, eludes simple identifications via isolated states [16]. The multichannel bound states in this region of the spectrum are likely to be of strongly mixed character. However the phenomenological description of the data described in Sec. III, when combined with the theoretical analysis summarized by Figs. 7 and 8 gives rise to a high degree of confidence in the assignment of the underlying symmetry labels in Table I. Although all symmetry labels for near-threshold detuning are approximate, these tend to correlate with case (c) symmetry labels for detunings far from threshold. A coupled channel dynamics calculation of both ground and excited states would be required to provide a deeper basis of understanding. Such an approach may be able to reconcile the much more complex trap-loss spectrum.[6]

VI. CONCLUSION

We report a photoassociation spectrum for ${}^{87}\mathrm{Rb}$ in the region where molecular states recouple into the eight hyperfine dissociation limits from the interaction ${}^{87}\mathrm{Rb}(5p_{3/2}) + {}^{87}\mathrm{Rb}(5s_{1/2})$. The photoassociation events recorded here preselect states which favor formation of bound ground-state molecules. This fact and the onset of predissociation above the ${}^{87}\mathrm{Rb}(5p_{3/2}) + {}^{87}\mathrm{Rb}(5s, f_b=1)$ asymptotes simplify the photoexcitation spectrum of cold collision pairs. An assignment of empirical potential-energy curves to two of the vibrational bands observed is made. The resulting potential-energy curves are consistent with those predicted by theory. Nevertheless numerous finer details in the spectrum remain to be identified. We currently attempt to explore these in studies at higher experimental resolution and better signal-to-noise ratio.

ACKNOWLEDGMENTS

We acknowledge support by the Sonderforschungsbereich 276 (TP C16) of the German Science Foundation. C.J.W. and P.S.J. acknowledge partial support from the U.S. Office of Naval Research.

[5]Based on the predicted enhancement of the free-bound absorption cross section at energies near the classical right-hand turning point, we can exclude significant contributions to our spectrum from PA events of the ground-state collision pairs $(5s, f_a=2) + (5s, f_b=1)$ and $(5s, f_a=1) + (5s, f_b=1)$. These collision pairs are also present in the trap, but photoexcitation from these combinations to attractive states at long range will appear at shorter wavelengths than those chosen here.

[6]Unpublished experimental and theoretical results on Na trap loss spectra by the NIST group support this contention.

[1] W.C. Stwalley, Y.H. Uang, and G. Pichler, Phys. Rev. Lett. **41**, 1164 (1978).
[2] E. Tiesinga, C.W. Williamsa, P.S. Julienne, K.M. Moses, P.D. Lett, and W.D. Phillips, J. Res. Natl. Inst. Stand. Technol. **101**, 505 (1996).
[3] C.C. Tsai, R.S. Freeland, J.M. Vogels, H.M.J.M. Boesten, B.J. Verhaar, and D.J. Heinzen, Phys. Rev. Lett. **79**, 1245 (1997).
[4] A. Fioretti, D. Comparat, A. Crubellier, O. Dulieu, F. Masnou-Seeuws, and P. Pillet, Phys. Rev. Lett. **80**, 4402 (1998).
[5] T. Takekoshi, B.M. Patterson, and R.J. Knize, Phys. Rev. Lett. **81**, 5105 (1999).
[6] T. Takekoshi, B.M. Patterson, and R.J. Knize, Phys. Rev. A **59**, R5 (1999).
[7] A.N. Nikolov, E.E. Eyler, X.T. Wang, J. Li, H. Wang, W.C. Stwalley, and P.L. Gould, Phys. Rev. Lett. **82**, 703 (1999).
[8] C. Gabbanini, A. Fioretti, A. Lucchesini, S. Gozzini, and M. Mazzoni, Phys. Rev. Lett. **84**, 2814 (2000).
[9] C.M. Dion, D. Drag, O. Dulieu, B.L. Tolra, F. Masnou-Seeows, and P. Pillet, Phys. Rev. Lett. **86**, 2253 (2001).
[10] A. Fioretti, C. Amiot, C.M. Dion, O. Dulieu, M. Mazzoni, G. Smirne, and C. Gabbanini, Eur. Phys. J. D **15**, 189 (2001).
[11] C.W. Williams, E. Tiesinga, and P.S. Julienne, Phys. Rev. A **53**, R1939 (1996).
[12] M. Movre and G. Pichler, J. Phys. B **10**, 2631 (1977).
[13] S. Wolf and H. Helm, Phys. Rev. A **62**, 043408 (2000).
[14] M. Prevedelli, T. Freegarde, and T.W. Haensch, Appl. Phys. B **60**, 241 (1995).
[15] M. Erhard and H. Helm, Phys. Rev. A **63**, 043813 (2001).
[16] C.J. Williams and P.S. Julienne, J. Chem. Phys. **101**, 2634 (1994).
[17] R.J. LeRoy and R.B. Bernstein, J. Chem. Phys. **52**, 3869 (1970).
[18] J. Weiner, V.S. Bagnato, S. Zilio, and P.S. Julienne, Rev. Mod. Phys. **71**, 1 (1999).
[19] B. Bussery and M. Aubert-Frecon, J. Chem. Phys. **82**, 3224 (1985).
[20] P.S. Julienne and J. Vigue, Phys. Rev. A **44**, 4464 (1991).
[21] P.S. Julienne, J. Res. Natl. Inst. Stand. Technol. **101**, 487 (1996).
[22] C. Boisseau, E. Audouard, J. Vigue, and P.S. Julienne, Phys. Rev. A **62**, 052705 (2000).
[23] J. Bohn and P.S. Julienne, Phys. Rev. A **60**, 414 (1999).
[24] M. Machholm, P.S. Julienne, and K.-A. Suominen, Phys. Rev. A **64**, 033425 (2001).
[25] E.G.M. van Kempen, S.J.J.M.F. Kokkelmans, D.J. Heinzen, and B.J. Verhaar, Phys. Rev. Lett. **88**, 093201 (2002).